This is still quite a bit larger than the value to be expected if the cavity fluid could be removed (case a).

From a practical point of view, one would control the rate of cleaning by exercising some control over the characteristics of the brush or jet-spray apparatus that is typically used in surface cleaning. As our model demonstrates, it is the shear stress exerted by the brush- or jet-driven flow across the cavity surface that affects the rate of removal of a contaminant. This shear stress appears in the model only in the Peclet number (Eq. [9]).

Our earlier work (1) predicts that in the range of Peclet numbers of likely occurrence (say $\geq 10^3$-10^5), convection aids removal by a factor E which is linearly and inversely proportional to Peclet number, *i.e.*

$$E \sim \mathrm{Pe}^{-1} \qquad [25]$$

Thus, all other physical and geometrical parameters remaining the same, the removal time is reduced by a factor that is linear in shear stress S_0. In a brush cleaner, the shear stress may be controlled through the rotational speed of the brush as well as the proximity of the brush to the surface to be cleaned. In a jet-spray apparatus, the dynamics are more complex, and depend upon the jet velocity and the proximity and orientation of the jet with respect to the target surface. The mathematical model illustrated here should be useful to those concerned with the design, improvement, and utilization of cleaning systems, when used in conjunction with appropriate laboratory studies of the cleaning of real surfaces.

Conclusions

A mathematical model has been formulated with which one can assess the time scales associated with removal (by convection-aided diffusion and/or by a neutralization reaction) of a chemical contaminant from a small cavity in a surface. Idealizations of the geometry make solutions possible via relatively simple numerical methods. In principle, more complex geometries and external flows could be considered, but at considerable increase to the cost of computation.

For a fluid hydrodynamically trapped within a cavity, but capable of circulation induced by the external flushing flow, the time for removal of a diffusible contaminant is strongly dependent on circulation within the cavity. The degree of effectiveness of circulation, and the effectiveness of a neutralization reaction, can be assessed using the models presented here.

Acknowledgment

Numerical computations were supported by the Army Research Office under its contract DAAG29-80-K-0058. We gratefully acknowledge this support.

Manuscript submitted Sept. 7, 1983; revised manuscript received Dec. 19, 1983.

LIST OF SYMBOLS

A aspect ratio (H/L)
$C_T(C_D)$ concentration of toxic (detoxifying) species (mol/cm^3)
$\mathfrak{D}$ diffusivity in the cavity liquid (cm^2/s)
D dilution ratio (cavity volume/cleaning fluid volume)
E enhancement ratio
$E1$ enhancement factor for chemical reaction
H depth of cavity (cm)
k specific reaction rate (cm^3/mol-s)
K dimensionless reaction rate constant ($kC_{T_0}L^2/\mathfrak{D}$)
L length of cavity (cm)
Pe Peclet number, ($S_0L^2/\mu\mathfrak{D}$)
R concentration ratio (C_{D_∞}/C_{T_0})
Re Reynolds number ($\rho u_c L/\mu$)
Sc Schmidt number (ν/D_T)
S_0 shear stress at $y = A$ (dyn/cm^2)
t time (s)
u velocity vector (cm/s)

Greek Letters

μ viscosity of cavity liquid (poise)
ξ fractional conversion

REFERENCES

1. R. Chilukuri and S. Middleman, *Chem. Eng. Commun.*, **22**, 127 (1983).
2. R. Chilukuri, Ph. D. Thesis, University of California, San Diego, La Jolla, CA (1982).
3. R. B. Bird, W. E. Stewart, and E. N. Lightfoot, "Transport Phenomena," John Wiley and Sons, Inc., New York (1960).

Electroluminescence and Photoluminescence of GaAs in Aqueous Redox Electrolytes

Franco Decker,* Milton Abramovich, and Paulo Motisuke

Instituto de Fisica, UNICAMP, Campinas, Sao Paulo, Brazil

ABSTRACT

Spectral resolved electroluminescence has been observed for n-GaAs in the presence of different hole injecting redox electrolytes from 0.8 to 1.25 μm. Photoluminescence spectra were obtained for n-GaAs in the same electrolytes. Luminescence was observed both in bandgap and subbandgap energy ranges. The presence of a deep acceptor level, attributed to Ga vacancies, is inferred. Efficient charge transfer to this level and/or to the valence band can be observed with a suitable choice of the redox electrolyte.

The occurrence of hole injection from a redox electrolyte into the valence band and/or into an intermediate level (deep level and/or surface state), of a semiconducting electrode can be detected via electroluminescence (EL). This phenomenon has been observed with the one-electron redox injecting electrolyte $Fe(CN)_6^{3-/4-}$ for GaP (1, 2), and more recently for GaAs by Decker *et al.* with the couples $Fe^{2+/3+}$, $Ce^{3+/4+}$, $Fe(CN)_6^{3-/4-}$ (3). In that work, the mechanism of hole injection was elucidated by the use of the rotating ring-disk technique as well as by electroluminescence. Ring-disk results that are in excellent agreement with the ones in Ref. (3) were also published by Menezes and Miller (4). The electroluminescence measurements reported in Ref. (3) were not spectrally resolved because of instrumental limitations. The present publication is, therefore, mostly devoted to the investigation of the EL spectra up to 1.25 μm, of the relationship between the spectra and the redox electrolyte used, and to the comparison with photoluminescence (PL) spectra of GaAs. Interesting comparisons can be made with previous works on EL from GaAs (5) and from II-VI binary and ternary compounds (6-9). In those papers, the injecting species was a highly active intermediate, like OH ·

*Electrochemical Society Active Member.

Key words: semiconductor/electrolyte junctions, luminescence.

or SO_4^- ·, resulting from the reduction of peroxide or persulfate. The energy-level distribution of such an injecting species is poorly defined, and therefore little information on the energy level at which the hole-injection process takes place can be extracted from the spectra. Using one-electron redox couples like $Fe^{2+/3+}$, $Ce^{3+/4+}$, $Fe(CN)_6^{3-/4-}$, on the contrary, the energetic conditions for hole injection into the valence band or into some intermediate level of GaAs can be analyzed more carefully. Moreover, the use of a redox ion as a hole injecting species allows a steady-state measurement of an EL spectrum, once the mass transport of the electrolyte to the electrode surface is well defined. In practice, this procedure can be employed only if the surface conditions of the electrode do not change too much during the measurement. If drastic changes occur (like from an oxide-coated to a hydride-coated surface) quenching of radiative recombination can take place and a distorted and weaker spectrum results. It is therefore very important to control the electrode potential during EL measurements, since adequate electron concentration at the semiconducting electrode surface has to be maintained. At the same time, side reactions giving H_2 evolution have to be avoided.

Very large cathodic potentials can induce either hole injection due to high concentration of intermediates (10, 11) or ion injection and migration (12, 13) into the semiconducting electrode. Both phenomena can cause luminescence; high cathodic polarization has therefore been avoided in our work in order to confine our study to EL resulting from hole injection by the redox electrolytes.

Experimental Techniques

Electroluminescence.—The use of redox ions in low (10^{-3}–$10^{-2}M$) concentration as the hole injecting species requires an efficient stirring of the electrolyte, in order to guarantee diffusion-controlled hole injection and current high enough to yield detectable EL signals. In Ref. (3) the rotating disk technique was used in order to guarantee efficient mass transport and constant current. Here, this technique is impractical because the image of the rotating electrode onto the spectrometer slit is unstable, causing fluctuations of the detected EL signal. Stirring by means of magnetic stir-bars or other mechanical devices produces enormous oscillations in the hole-injection current and therefore in the EL intensity as well. The best configuration has been found to be an electrolyte jet impinging onto a stationary electrode, the electrolyte flux being sustained by an all-Teflon rotary pump that fills an intermediate reservoir (Fig. 1). The electrolyte level in this reservoir is constantly kept ~10 cm higher than that in the main cell, to which the electrolyte flows simply by gravity. EL intensity fluctuations of a few percent and even smaller current oscillations have been achieved in this way. The GaAs electrode is set in front of the nozzle (with 1-2 mm separation) and sideways to the cell flat Pyrex window, so that the image of its front edge can be focused onto the spectrometer slit. The EL originating from the flat-crystal surface exposed in front of the nozzle can also contribute to the signal as long as defocusing is not too severe. The optical setup consists of a collecting lens, a long pass filter with cutoff at 0.7 μm, a Spex spectrometer, and a S-1 EMI photomultiplier. The spectral sensitivity of the photomultiplier decays very steeply for λ greater than 1.1 μm. Consequently, the photomultiplier relative spectral response was compared to that of a flat photoacoustic photodetector, and correction factors were derived for wavelengths in the range 0.7-1.25 μm. The photomultiplier was cooled with liquid air in order to achieve maximum signal-to-noise ratio. The slit widths of the spectrometer were kept at 1.0 mm in most experiments, which brings a spectral resolution of 16Å at λ = 1.0 μm. Measurements of EL for λ greater than 1.3 μm were not possible with the present experimental setup both because of photomultiplier insensitivity and because of strong IR absorption in the aqueous electrolyte. A different setup will be assembled for EL measurements in this IR region.

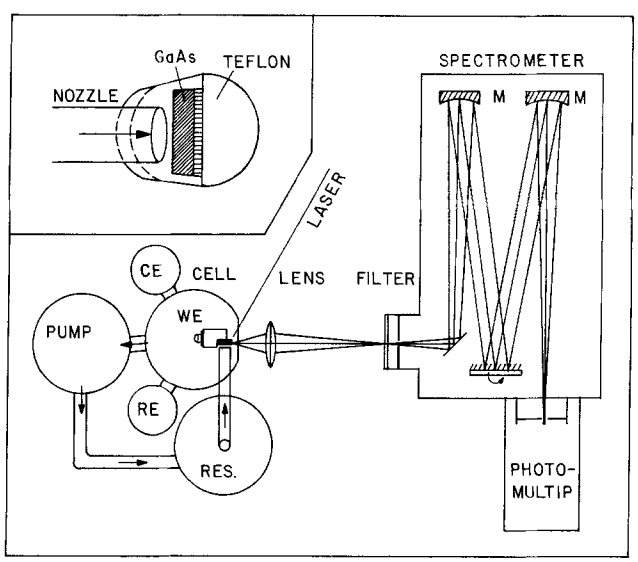

Fig. 1 Top view of the experimental setup for photoluminescence and electroluminescence. The inset shows the electrode mounting in detail (side view).

The electronic apparatus consisted of conventional potentiostat and programmer, voltmeter, electrometer, and a double-pen strip-chart recorder. The EL and PL spectra were obtained by driving the spectrometer at the constant speed of 5 Å s^{-1}. The electrochemical cell and the reservoir were made of Pyrex and connected to each other and to the pump by Tygon tubes. The three-electrode configuration was always used, and all potentials will be referred to the saturated calomel reference electrode (RE). The electrolytes were prepared with triply distilled H_2O and with high purity reagents. The presence of oxygen did not affect our measurements; therefore, it was unnecessary to deaerate the electrolytes. Graphite was used as the counterelectrode (CE). An n-GaAs sample from Laser Diode Company, doped with a Si concentration at 5×10^{17} cm^{-3}, was used as the working electrode (WE). The ohmic contact was obtained by the evaporation of Sn followed by annealing under N_2 atmosphere during 2 min at 400°C. The sample was mounted on a Teflon rod (as shown in Fig. 1) with the crytallographic (100) face exposed to the solution. The semiconductor surface was etched in H_2SO_4:H_2O_2 (1:1 by volume) prior to use.

Photoluminescence.—The same setup described for EL was used for the PL measurements. The photoexcitation was made by means of a 3 mW He-Ne laser from Spectra Physics focused on GaAs front crystal edge. In this way, the same alignment for PL and EL could be used.

Experimental Results

Photoluminescence of GaAs.—PL of GaAs in air or vacuum has been widely studied for several years, as a function of temperature, doping, and various other parameters (14). It is well known that heat-treatments and surface contamination may affect PL. First, we ran the photoluminescence spectrum at room temperature and in air of GaAs sample as received from the factory, with mirror-like surface finishing. The spectrum (not corrected for photomultiplier sensitivity) is labeled as PL° in Fig. 2: a very strong band-to-band transition is observed in 0.87 μm, and a weaker and much broader band shows up around 1.1 μm (note the 30-fold increase in sensitivity in the IR region).

PL and EL in $Fe(CN)_6^{3-}$ pH 13.—The GaAs electrode was assembled as previously shown, etched, and introduced into the electrochemical cell filled with a 30 mM $K_3Fe(CN)_6$ + 0.1M KOH electrolyte. This electrolyte composition was chosen because it is well known that

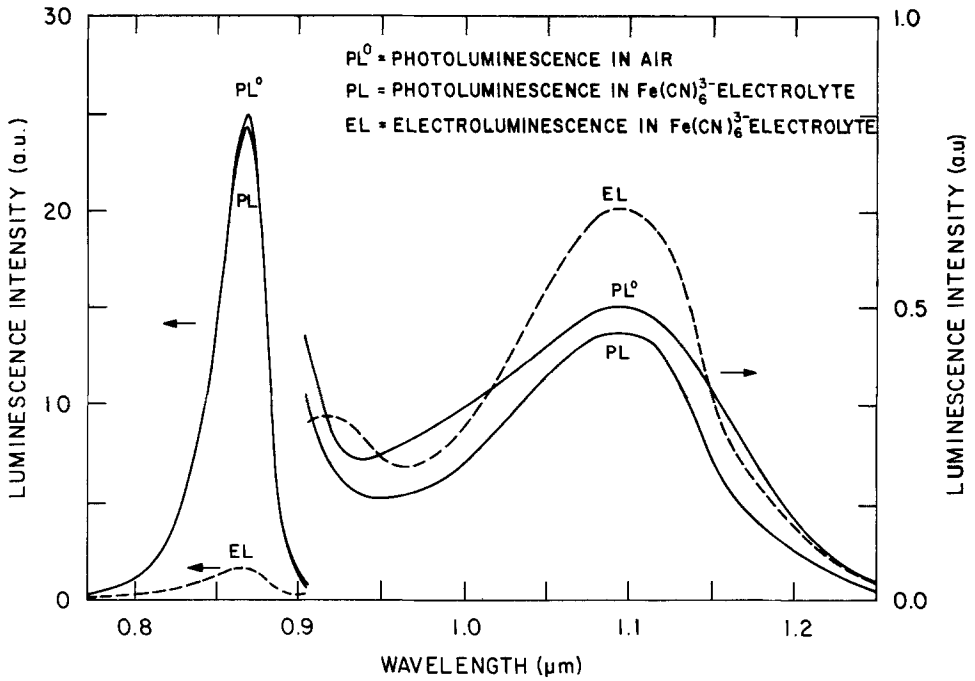

Fig. 2. Uncorrected photoluminescence (solid lines) and electroluminescence (dashed lines) spectra of n-GaAs in air (PL°) and in aqueous 0.03M $K_3Fe(CN)_6$ + 0.1M KOH electrolyte (PL and EL). During PL, the GaAs electrode was held at open circuit; during EL, at −1.75V.

$Fe(CN)_6^{3-}$ injects holes into GaAs in alkaline solutions (3, 4, 15). The PL spectrum (Fig. 2) was obtained with no potential applied to the GaAs electrode. This spectrum is virtually identical to the one obtained in air in the band-to-band region, and shows only minor changes in the IR. It is therefore clear that none of the features observed in the photoluminescence spectra depends on contact with the electrolyte, *i.e.*, the electrolyte ions have no specific effect on PL. When potential is applied to the electrode, and the laser switched off, luminescence from the electrode appears as soon as a cathodic current flows in the cell (Fig. 3). At −1.75V, the EL intensity is maximum and very stable in time at all wavelengths (see Fig. 4). Therefore, a steady-state EL spectrum (shown in Fig. 2) was obtained at a constant −1.75V potential. In the EL spectrum both bands at 0.87 and 1.1 μm are observed; however, the intensity of the 0.87 μm band is now much weaker than that observed in PL. A better analysis of the PL and EL spectra can be made after multiplying the measured intensities by the correction factors and after normalization to the same peak height at 0.87 μm. This is shown in Fig. 5. The band-to-band recombination spectrum in the EL is broader than in the PL (see Table I), which is mainly due to the enhancement of the short wavelength side of the peak. In the IR region, the emitted intensities level off in both spectra; however, the ratio of this intensity to that in 0.87 μm is much larger in the EL spectrum than that in PL. It is unfortunate that the photomultiplier is so insensitive for wavelengths greater than 1.25 μm and therefore that the long wavelength tail of the IR peak cannot be seen with this experimental setup. A structure is seen at 0.93 μm in EL, but since it did not appear in all EL measurements, we shall not discuss it.

The complete dependence of EL with electrode potential at constant wavelength is shown in Fig. 3. EL appears

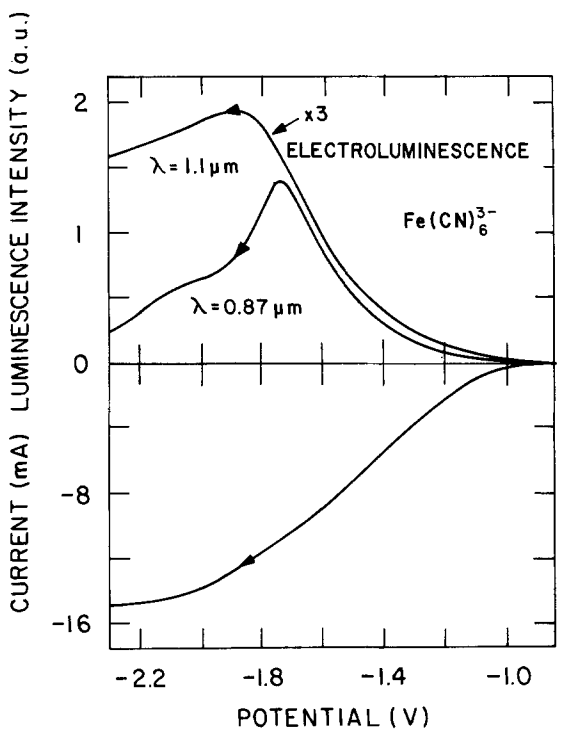

Fig. 3. Current-potential curve for n-GaAs in aqueous 0.03M $K_3Fe(CN)_6$ + 0.1M KOH in the dark (lower part). The corresponding EL intensities recorded as a function of applied potential for two different wavelengths are shown in the upper part. Note the three-fold increase in sensitivity for EL in λ = 1.1 μm. The potential was swept at a constant rate of −20 mV s^{-1}.

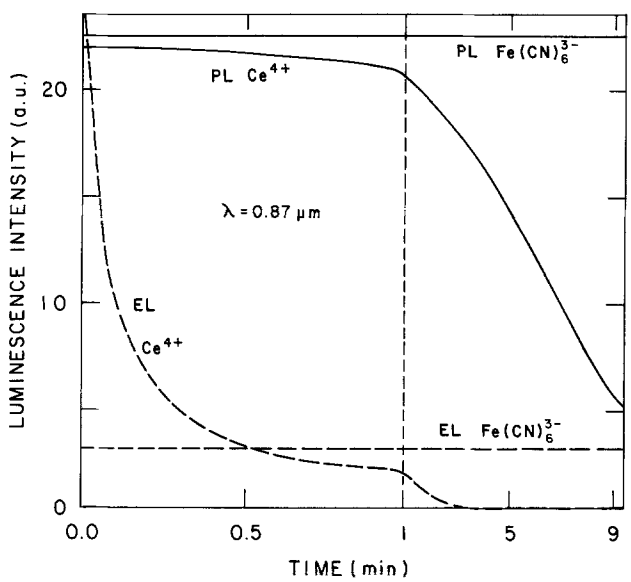

Fig. 4. Time dependence of PL (solid lines) and EL (dashed lines) of n-GaAs in 0.03M $K_3Fe(CN)_6$ + 0.1M KOH and in 0.03M $Ce(SO_4)_2$ + 1.0M H_2SO_4. At t = 0, either the laser was switched on (PL), or the electrode potential was stepped from 0 to −1.75V (EL).

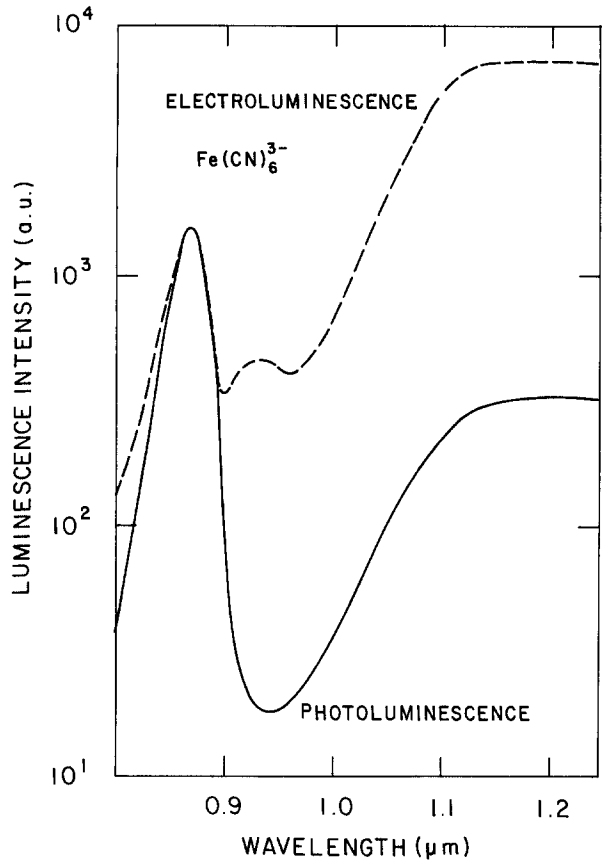

Fig. 5. PL (solid line) and EL (dashed line) spectra of n-GaAs after correction for photomultiplier efficiency and normalization to the same peak height in 0.87 μm. Electrolyte and polarization conditions are the same as in Fig. 2.

only with cathodic currents, starting for $V < -1.0$V. This is in agreement with previous observations (3), which were confined, however, to $\lambda < 0.9$ μm. For potentials more cathodic than −1.8V, EL at $\lambda = 0.87$ μm is quenched abruptly while EL at $\lambda = 1.1$ μm decays slowly and eventually becomes constant.

PL and EL in Fe^{3+} and Ce^{4+}, pH 0.—Electrolytes with 0.03*M* Fe^{3+} or 0.03*M* Ce^{4+} in 1.0*M* H_2SO_4 were used because the equilibrium potentials of these couples are located either in the GaAs bandgap ($Fe^{2+/3+}$) or overlap with the GaAs valence band ($Ce^{3+/4+}$).

A number of experimental difficulties arise, however, in acid electrolytes. Although the potential dependence of PL and EL was observed to be similar to that observed at pH 13 (with the exception of a 0.6V shift in the onset of EL), no electrode potential could be found at which EL would be stable during the time required to measure a complete spectrum. PL intensities at fixed wavelength and potential decrease with time, contrary to what occurs in 0.1*M* KOH. The variation of PL and EL intensities with time are shown in Fig. 4 for Ce^{4+} and Fe $(CN)_6^{3-}$. An exchange of Ce^{4+} by Fe^{3+} showed a similar decrease in PL and EL intensities with time.

It became clear to us that photocorrosion takes place at the laser spot on the GaAs electrode and the corrosion products are not dissolved quickly enough at pH 0. Corrosion products like gallium oxides are probably left on the surface [see also Ref. (16)], resulting in PL quenching. In fact, moving the laser spot to another region of the electrode restores the initial intensity of PL.

In order to measure EL, we had to apply the same technique previously employed by Ellis *et al.* (6, 7) which consists in short (2s) forward-bias pulses alternated by longer (20s) time intervals in which the GaAs-electrolyte junction is reverse biased. At the same time, the spectrometer was driven at constant speed. The two EL spectra, relative to Fe^{3+} or Ce^{4+} ions in the same 1*M* H_2SO_4 support

Table I. Characteristics of the luminescence spectra of n-GaAs grown from the melt in the bandgap region (first two columns) and ratios between the luminescence intensities, corrected by photomultiplier efficiency, at 0.87 and 1.1 μm (third column)

	Peak position (Å)	Bandwith FWHM (Å)	$\frac{I_{0.87}}{I_{1.1}}$
PL° in air	8700	343	6.24
PL in $K_3Fe(CN)_6$ + KOH	8700	345	6.71
EL in $K_3Fe(CN)_6$ + KOH	8680	392	0.30
EL in $Ce(SO_4)_2$ + H_2SO_4	8680	390	0.35
EL in $Fe_2(SO_4)_3$ + H_2SO_4	8660	408	0.08

electrolyte, are shown in Fig. 6. It is important to notice that the spectra were obtained one after the other without removing either the cell or the electrode. The redox electrolyte was substituted, and otherwise the same experimental conditions were maintained, so that the EL intensities of both spectra can be directly compared. The following remarks are important: (*i*) the EL with Ce^{4+} is more intense than that with Fe^{3+}, by a factor of 10 in 0.87 μm and by a factor of only 2.2 in 1.1 μm (note the different scales in which EL intensities for Fe^{3+} and for Ce^{4+} are shown in Fig. 6) and (*ii*) in the Fe^{3+} EL spectrum, the IR peak is more intense than the peak in 0.87 μm.

The more relevant data from PL and EL spectra in the three electrolyte are summarized in Table I.

Discussion and Conclusions

The PL and EL spectra give a valuable insight into processes related to radiative recombination and charge transfer across the semiconductor-electrolyte interface. The band-to-band recombination emission spectrum of the n-GaAs with maximum at ~0.87 μm is observed in PL as well as in EL, but in the latter the spectrum appears slightly broader and its peak is shifted to shorter wavelength, as shown in Fig. 5 and Table I. Since this broadening occurs almost exclusively in the high energy tail we attribute the difference to self-absorption effects, *i.e.*, on average, EL is produced nearer to the GaAs-electrolyte interface than PL. Similar conclusions about EL spectra broadening were drawn by Ellis *et al.* (6); they compared EL and PL spectra of cadmium-sulfo-selenide electrodes. This conclusion is valid for any material where the penetration depth α^{-1} of the exciting photons is of the same order, or greater than the diffusion length L of the injected minority carriers. In particular, for n-GaAs α^{-1} is ~0.3 μm (at $\lambda = 0.63$ μm) and L_p is of the same order of magnitude, as long as the hole lifetime is in the order of 10^{-9}s. The last hypothesis was not experimentally confirmed here but can be taken as reasonable, since at the semiconductor-electrolyte interface the surface recombination velocity is high (17).

The subbandgap emission bands with its maximum at ~1.1 μm, uncorrected to photomultiplier spectral response, are also observed in PL and EL on samples grown from the melt. However, samples grown by us by liquid phase epitaxial (LPE) technique showed no measurable PL signal in this subbandgap spectral region, although a similar laser beam was used to induce bandgap emission of the same intensity as above. Both LPE and melt-grown samples are doped only with Si. However, the LPE samples have a lower density of defects, in particular Ga vacancies, than the crystals grown from the melt. Since there is a good agreement between the energetic position of the subbandgap peak observed by us with that cited in the literature on photoluminescence of GaAs (18), we attribute the 1.1 μm emission band to radiative transition from shallow donor states to deep acceptor states created by gallium vacancies. In the following, only n-GaAs grown from the melt will be considered. As shown in Fig. 2, the spectra of PL with the sample immersed in electrolyte or in air are almost identical, *i.e.*, the electrolyte ions have no specific effect on PL. However, the overall intensities in EL as well as in PL may decrease

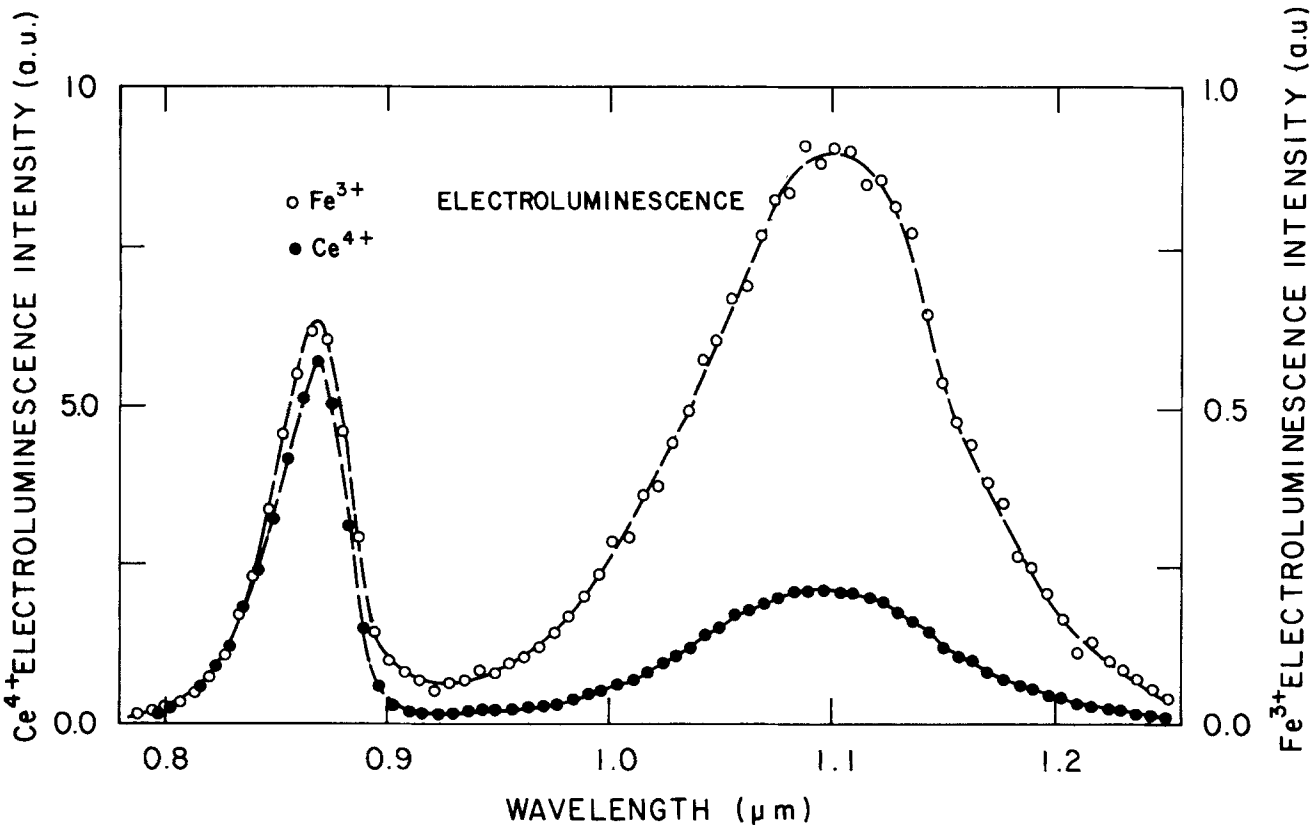

Fig. 6. Uncorrected EL spectra of n-GaAs in 0.01M $Fe_2(SO_4)_3$ + 1.0M H_2SO_4 and in 0.03M $Ce(SO_4)_2$ = 1.0M H_2SO_4. The electrode potential was continuously pulsed between 0 (20s) and −1.75V (2s), while the emission spectrum was scanned at 5 Å s^{-1}. Note the tenfold increase in sensitivity in order to record the spectrum in the $Fe_2(SO_4)_3$ electrolyte.

in time, with a time constant depending on the electrolyte composition (see Fig. 4). The photoluminescence quenching in the presence of the electrolyte was attributed to electrode-surface degradation due to photocorrosion effects, which, in fact, can be observed with the naked eye.

The most remarkable difference between PL and EL spectra is the variation of the ratio between the near-bandgap emission peak intensity to the subbandgap emission intensity ($I_{0.87}/I_{1.1}$). As shown in Fig. 5 and Table I, this ratio is smaller by a factor of 22 in EL than PL when the electrolyte is a solution of K_3 $Fe(CN)_6$ + KOH, and by a factor of 78 when the electrolyte is changed to $Fe_2(SO_4)_3$ + H_2SO_4. This variation can be due to one or more of the following:

1. The density of the acceptor centers is higher in the region near to the GaAs-electrolyte interface. Gallium vacancies, in particular, may have higher density closer to the surface as a consequence of corrosive reactions taking place at the interface.

2. The band-to-band radiative transition is quenched by a more competitive nonradiative recombination at the GaAs electrolyte surface.

3. The electron-transfer rate is larger at the intra-bandgap state energy (gallium vacancy state) than at the valence bandedge energy. We shall discuss this point in the following.

An energy-band diagram is sketched in Fig. 7 for the semiconductor-electrolyte interface, taking as 0.3 eV the distance of the acceptor level (E_{INT}) from the valence bandedge (E_{VB}) of GaAs. This value is in agreement both with the known energy position of gallium vacancies and with our corrected PL and EL spectra, which show a maximum around 1.2 μm (Fig. 5). In the electrolyte side, the unoccupied energy levels of Fe^{3+} and Ce^{4+} are depicted as gaussian distributions that have their maximum at an energy E_R above the Fermi level of the couple (taken as the redox potential). The rearrangement energy E_R is ~1.2 and ~1.5 eV for the Fe^{3+} and for Ce^{4+}, respectively, (19). The proper matching between electrodes and electrolyte energy levels is obtained knowing the flatband potential of GaAs, which nearly coincides with the conduction bandedge E_{CB} in our n-type samples. The value of −0.5 eV *vs.* NHE (pH = 0) was chosen for E_{CB}, in agreement with data from the literature (3, 4, 20). The unoccupied energy levels of $Fe(CN)_6^{3-}$ could also be included in the diagram, provided the shift with pH of the GaAs energy levels is taken into account. For the sake of simplicity, however, we shall consider in Fig. 7 only the energy level distributions corresponding to the Fe^{3+} and Ce^{4+} ions. Due to the redox potentials of the two couples, Ce^{4+} should easily inject holes into the valence band of GaAs, but Fe^{3+} should not. This was indeed confirmed by previous work (3, 4). Here, we did observe bandgap luminescence with Fe^{3+}, although ten times weaker than with Ce^{4+} (Fig. 6). Bandgap luminescence indicates unequivocally hole injection into the valence band. This can be attributed either to an underpotential reduction of Fe^{3+} by valence-band electrons and/or to an upper shift of the GaAs bandedges during the −1.75V potential pulse used in the present EL measurements. This pulse technique differs from the potential sweep technique used previously by Decker *et al.* (3), allowing higher EL intensities. From the EL measurements, and from Fig. 7, we conclude:

1. $Fe(CN)_6^{3-}$, Ce^{4+}, and Fe^{3+} inject holes both into the valence band and into the intra-bandgap state.

2. The ratio $I_{0.87}/I_{1.1}$ falls from 0.3 [Ce^{4+}, $Fe(CN)^{3-}$] to 0.08 (Fe^{3+}), indicating that the Fe^{3+} injects holes less efficiently into the valence band than the other electroactive species do.

3. The rate of hole injection for Ce^{4+} and $Fe(CN)_6^{3-}$ is comparable; for Fe^{3+} this rate is lower, both at E_{INT} and at E_{VB}.

Since the energy-level distribution in the electrolyte is very broad, a good overlap of both the deep level and the valence band with empty levels in the electrolyte occurs. Consequently, the electron transfer from the semiconductor to the redox ion can occur isoenergetically, the initial state being either at the valence bandedge or in the

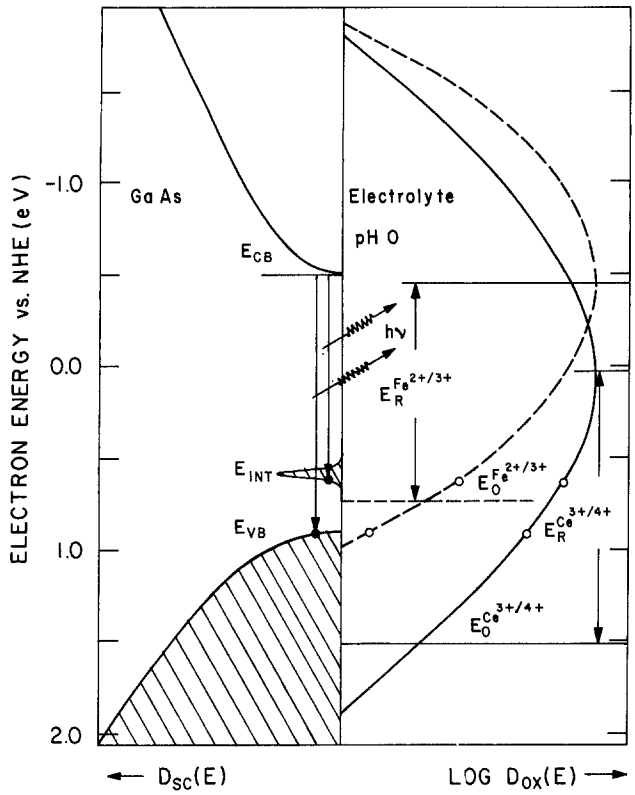

Fig. 7. Energy band diagram for the n-GaAs/redox electrolyte interface. In the semiconductor, the dashed areas represent filled states. E_{CB} and E_{VB} indicate the conduction and the valence band edges; E_{INT} is the energy of the deep level attributed to Ga vacancies. In the electrolyte, the solid and dashed parabolas represent the energy-level distribution of the empty Ce^{4+} and Fe^{3+} states, respectively. E_O represents the standard redox potentials, and E_R represents the so-called rearrangement energy for the redox couples. The following symbols are used to illustrate the electron transfer across the semiconductor/electrolyte interface. Filled dots: initial states. Open dots: final states. The vertical arrows in the GaAs indicate the radiative transitions taking place in the semiconductor after the electron transfer has occurred.

deep intra-bandgap level. In fact, the energy level model for the semiconductor-electrolyte interface (21) assumes isoenergetic charge transfer, since negligible phonon emission during electron transfer is expected (22). For a single level E, the charge transfer rate is proportional to the density of occupied states in the solid and of unoccupied states in the electrolyte. One can see from Fig. 7 that the density of empty states in the electrolyte is larger at E_{INT} than at E_{VB}. The electron transfer at E_{INT} is then kinetically favored, unless the density of states at the valence bandedge overwhelms the density of states at the intra-bandgap level. The small ratios $I_{0.87}/I_{1.1}$ we observed in electroluminescence indicate, indeed, high charge transfer rate at E_{INT}. Our experiments with Fe^{3+} and Ce^{4+} in H_2SO_4 indicate also that the competition between charge transfer to the intra-bandgap state and charge transfer to the valence band is regulated by the redox potential of the couple. As a general conclusion, electroluminescence in aqueous redox electrolytes is a technique sensitive per se to the presence of intra-bandgap states. This conclusion agrees well with previous results of EL measurements on GaP (1).

Finally, the charge transfer from the conduction band of GaAs cannot be excluded. In fact, Fig. 7 shows that the capture of conduction-band electrons can also occur at a high rate without violation of the principle of isoenergetic charge transfer. Indeed, simultaneous charge transfer to distinct energy levels is unavoidable with small bandgap semiconducting electrodes in the presence of aqueous redox electrolytes.

Acknowledgments

The financial support from FINEP and CNPq is gratefully acknowledged.

Manuscript submitted Sept. 29, 1983; revised manuscript received Jan. 4, 1984.

REFERENCES

1. K. H. Beckmann and R. Memming, *This Journal*, **116,** 368 (1969).
2. Y. Nakato, A. Tsumura, and H. Tsubomura, in "Photoeffects at Semiconductor-Electrolyte Interfaces," A. J. Nozik, Editor, p. 145, ACS Symposium Series, American Chemical Society, Washington, DC (1981).
3. F. Decker, B. Pettinger, and H. Gerischer, *This Journal*, **130,** 1335 (1983).
4. S. Menezes and B. Miller, *ibid.*, **130,** 517 (1983).
5. B. Pettinger, H. R. Schöppel, and H. Gerischer, *Ber. Bunsenges. Phys. Chem.*, **80,** 849 (1976).
6. H. H. Streckert, J. Tong, M. K. Carpenter, and A. B. Ellis, *This Journal*, **129,** 772 (1982).
7. H. H. Streckert, J. Tong, and A. B. Ellis, *J. Am. Chem. Soc.*, **104,** 581 (1982).
8. H. H. Streckert, B. R. Karas, D. J. Morano, and A. B. Ellis, *J. Phys. Chem.*, **84,** 3232 (1980).
9. H. H. Streckert, J. Tong, M. K. Carpenter, and A. B. Ellis, Proc. Electrochem. Soc. 82-3, 633 (1982).
10. D. J. Bernard and P. Handler, *Surf. Sci.*, **40,** 141 (1973).
11. H. Gerischer, N. Müller, and O. Haas, *J. Electroanal. Chem.*, **119,** 41 (1981).
12. M. A. Butler and D. S. Ginley, The Electrochem. Soc. Meeting, **79-2,** 1577 (1979).
13. M. A. Butler and D. S. Ginley, *Appl. Phys. Lett.*, **36,** 845 (1980).
14. "Proceedings of the Tenth International Symposium on Gallium Arsenide and Related Compounds," Albuquerque, New Mexico, Sept. 19-22, 1982, G. E. Stillman, Editor, Institute of Physics Conference Series no. 65 Bristol, England (1983); E. W. Williams and H. B. Bebb, in "Semiconductors and Semimetals," Vol. 8, R. K. Willardson, Editor, p. 321, Academic Press, New York (1972); V. Swaminathan, N. E. Schumaker, and J. L. Zilko, *J. Lumin.*, **22,** 153 (1981); A. Mircea-Roussel and S. Makran-Ebeid, *Appl. Phys. Lett.*, **38,** 1007 (1981).
15. H. Gerischer, *Ber. Bunsenges. Phys. Chem.*, **69,** 578 (1965).
16. V. A. Myamlin and Y. V. Pleskov, "Electrochemistry of Semiconductors," p. 99, Plenum Press, New York (1967).
17. A. Heller, in "Photoeffects at Semiconductor-Electrolyte Interfaces," A. J. Nozik, Editor, p. 57, ACS Symposium Series, American Chemical Society, Washington, DC (1981).
18. "Semiconductors and Semimetals," Vol. 8, R. K. Willardson, Editor, pp. 324, 359-373, Academic Press, New York (1972); V. Swaminathan, N. E. Schumaker, and J. L. Zilko, *J. Lumin.*, **22,** 153 (1981).
19. F. Willig and K. P. Charlé, *Faraday. Discuss.*, **74,** 9 (1982).
20. R. Memming, *Ber. Bunsenges. Phys. Chem.*, **81,** 732 (1977).
21. H. Gerischer, *Z. Phys. Chem. N. F.*, **27,** 48 (1961).
22. R. R. Dogonadze, A. M. Kuznetsov, and A. A. Cherenko, *Russ. Chem. Rev.*, **34,** 759 (1965).